Chapter-5

Effect of Al addition on Electrochemical behaviour of Sn-0.7Cu-xAl lead-free solders alloys in 3.5 wt. %NaCl solution

5.1. Introduction

The literature has observed that very few works on electrochemical corrosion behaviour of lead-free solder alloys have been reported. Therefore, the influence of Al addition on the electrochemical corrosion behaviour of Sn-0.7Cu solder alloy has been taken up in this investigation. The ternary solder alloys of Sn-0.7Cu-xAl (x=0,1,2 & 3 wt.%) was prepared by vacuum induction melting. The corrosion characterization of these alloys has been done by electrochemical impedance spectroscopy (EIS) and corrosion behaviour in neutral 3.5 wt.% NaCl solution. The microscopic characterization before and after the corrosion has been done by field emission scanning electron microscope (FE-SEM), energy dispersive x-ray analyzer (EDXA), and X-ray diffraction (XRD) and Optical Microscope (O.M.), aiming to find out the effect of variation of Al on microstructure and corrosion behaviour of Sn-0.7Cu.

5.2 Results and Discussion

5.2.1 Metallographic Analysis of Sn-0.7Cu-xAl solder alloys

Fig. 5.1 shows the SEM microstructure and EDS analyses of Sn-0.7Cu-xAl (x=0, 1, 2, and 3) lead-free solder alloys. It revealed three distinct phases, The Al_2Cu(IMC) black contrast particles, a dark grey area appearing as precipitation during Cu_6Sn_5(IMC) solidification, and a light grey phase β-Sn matrix phase[153]. In binary Sn-0.7Cu liquid alloy, nucleation occurs at around 227^0C (eutectic temperature) and is transferred to Sn-0.7Cu and β-Sn5 (L + Cu_6Sn_5/Cu_3Sn+ β-Sn). Solidified Cu6Sn5 and β-Sn are primarily supplemental in Sn–0.7Cu alloys. The dissolution of Cu_6Sn_5 occurs at a eutectic temperature, and the diffusion of β-Sn produces the eutectic Cu_6Sn_5. A small quantity of Al_2Cu precipitation phase has been observed in Sn–0.7Cu–xAl solder alloy. It may be due to the addition of 1 to 3 wt. % aluminum to the Sn–0.7Cu. β-Sn. Cu_6Sn_5 and Al_2Cu are the solidified Sn–0.7Cu–xAl alloy observed in the microstructure[154].

Fig. 5.1 depicts the microstructure of Sn–0.7Cu lead-free solder alloy with various aluminum concentrations. Fig. 5.1 (a)-(d), the Sn–0.7Cu microstructure consists of Cu_6Sn_5/Sn eutectics and β-Sn. The BSE microstructure of the lead-free solder alloy Sn–0.7Cu is refined by adding a small quantity of aluminum, as illustrated in Fig. 5.1(a). Due to the dissolution of Al atoms into β-Sn and eutectic refining within the Sn–Cu–xAl alloys, Cu_6Sn_5/Sn and β-Sn eutectic phase become more even with increasing aluminum content. In Sn–0.7Cu–Al solder alloys, the black spots are the Cu agglomeration and the Al segregation [133].

The BSE microstructure of Sn–0.7Cu lead-free solder alloy and Sn-0.7Cu-xAl alloys are slightly different. Morphologies are altered by adding 1 to 3wt.% aluminum. The microstructure consists of the dispersion of the particles of Cu_6Sn_5/δ-Al_2Cu in the matrix of β-Sn, and at the boundary of β-Sn. The light grey zone is rich in Sn, whereas the dark grey is rich in Cu and Sn, and the black portion is rich in Al. It is inferred from the EDS results in table 5.1. As a result, the Al concentration in the IMC of Sn–0.7Cu–1Al and Sn–0.7Cu–2Al systems is substantially lower than that of the Sn–0.7Cu-3Al system. The concentration of Sn is inversely proportional to the concentration of Al[138]. Because of the chemical reaction between Sn, Cu, and Al, the thickness of IMC grows as the aluminum content increases, and the scalloped shape of IMC degrades and flattens. Cu_6Sn_5 is precipitated while solidifying Sn–0.7Cu, and Al with higher activity than Sn is preferentially responsive to Cu and causes δ-Al_2Cu phase development and Cu_6Sn_5 suppression [155]. Al and Cu atoms create the δ-Al_2Cu phase in Sn–0.7Cu–xAl solder alloys. Cu_6Sn_5 phase has been precipitation and is separated on the β-Sn boundary in Sn–0.7Cu-xAl. However, The effect of a 1-3wt% Al addition on IMC thickness is limited. Despite this, the brittle and thin interfacial IMC is suitable for vibration, impact resistance, and bonding strength between the solder substrate [15]. The mechanical

properties of the Sn–Cu–Al alloy are dominated by the morphologies and fluctuations of the interfacial IMC.

The experiment was performed with XRD, and the results are presented in Fig. 5.2. It can be seen that Sn-0.7Cn, Sn-0.7Cu-1Al, Sn-0.7Cu-2Al, and Sn-0.7Cu-3Al consist of the pattern of Cu_6Sn_5, β-Sn, and some δ-Al_2Cu peaks and are shown for the variation of aluminum in Sn-0.7Cu.

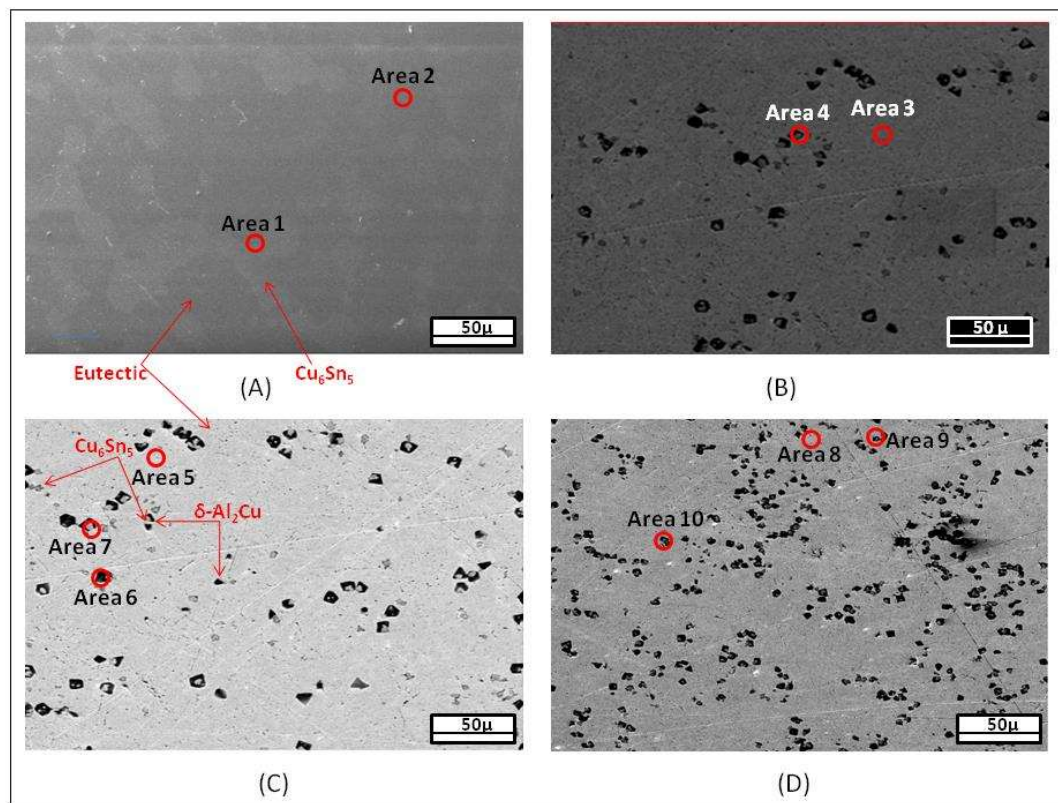

Fig.5. 1BSE Microstructure of non-corroded of *Sn-0.7Cu-xAl* solder alloys (a) x=0, (b) x=1, (c) x=2 and (d) x=3.

Table 5. 1 EDS analysis Results of areas 1-10 in Fig. 5.1

Area	Chemical Elements (Weight %)		
	Sn (L)	Cu (K)	Al (K)
Area 1	99.49	00.51	-
Area 2	97.86	02.14	-
Area 3	100.0	-	-
Area 4	30.30	40.0	29.60
Area 5	100.0	-	-
Area 6	45.36	15.7	38.94
Area 7	94.60	-	05.40
Area 8	100.0	-	-
Area 9	75.10	16.8	8.10
Area 10	18.50	-	81.50

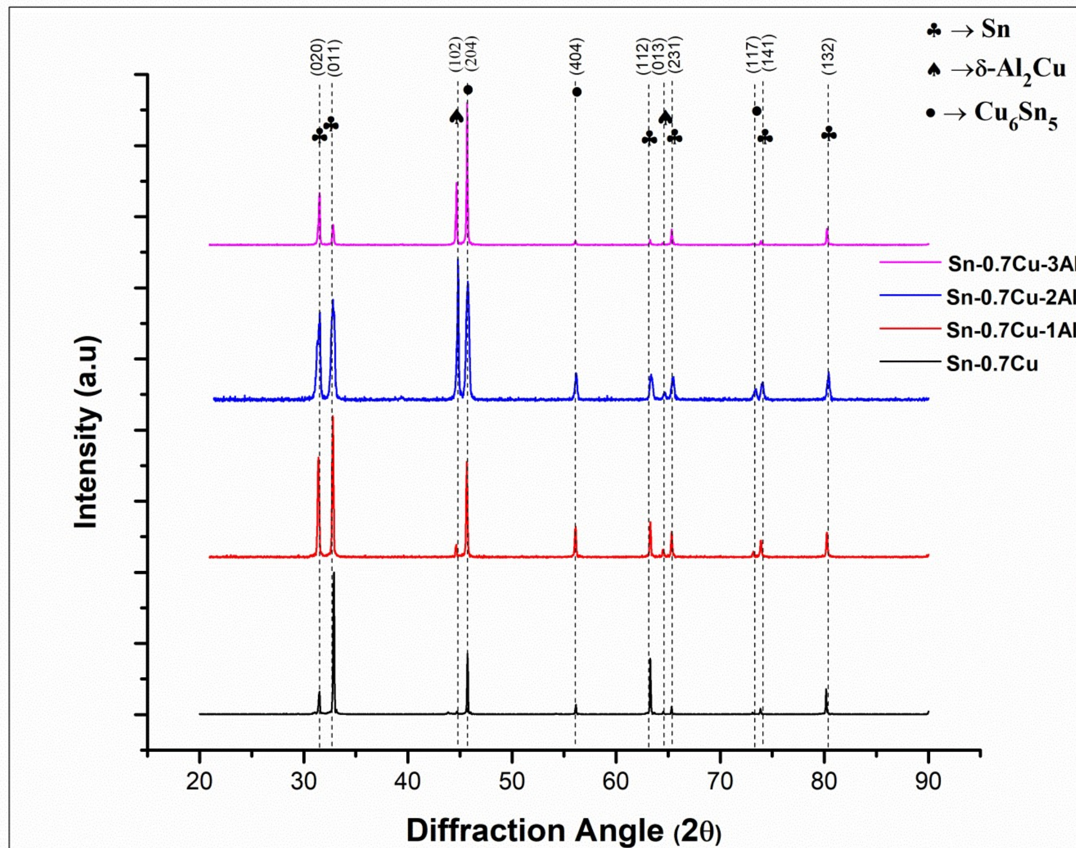

Fig.5. 2 XRD pattern of the non-corroded Sn–0.7Cu–xAl lead-free solder alloys

5.2.2 Immersion Test

The rate of corrosion of Sn-0.7Cu-xIn alloys was assessed non-electrochemically using the traditional weight loss/gain approach. This method is used to calculate the loss of a metal due to corrosion by exposing a metal specimen of a specified area to a corrosive environment for a given time interval and calculating the weight difference before and after exposure. The most often used method of describing corrosion rate is millimeters per year (mm/yr). The formula is used to calculate the rate of corrosion.

$$CPR = \frac{KW}{\rho At}$$

Where K = constant and a value of 87.6 is taken as a present case.

W = Weight loss in grams

ρ = density of specimen in grams per cubic centimeter

A = expose area in a square centimeter

t = exposure time in an hour

The weight loss experiment of Sn-0.7Cu-xIn samples immersed in 3.5wt. % NaCl lasted 24 weeks, and the results are presented in Fig. 4.4.

Up to 20 weeks, all of the samples demonstrated ongoing weight decrease. The binary Sn-0.7Cu solder alloy has seen the most weight reduction, whereas the ternary Sn-0.7Cu-xIn alloys experienced the least. A slight weight change can be seen in all of the samples after 8 weeks, which might be attributable to the formation of the oxide layer.

Fig. 4.5 shows cumulative weight loss after 24 weeks of exposure. It shows that 1wt.% Al solder alloys show the least (7.02 ± 0.017) x 10^{-4} mm/yr, and binary Sn-0.7Cu alloys show the highest corrosion rate (9.26 ± 0.0062) x 10^{-4} mm/yr.

Table 5. 2 Weight change of Sn-0.7Cu-xAl alloys after immersion in 3.5wt.% NaCl Solution.

Times (Weeks)	Weight Loss (mg)			
	Al(x=0)	Al(x=1)	Al(x=2)	Al(x=3)
8	0.455	0.351	0.391	0.413
12	0.486	0.396	0.414	0.424
16	0.545	0.411	0.443	0.464
20	0.571	0.437	0.485	0.526
24	0.585	0.483	0.501	0.531

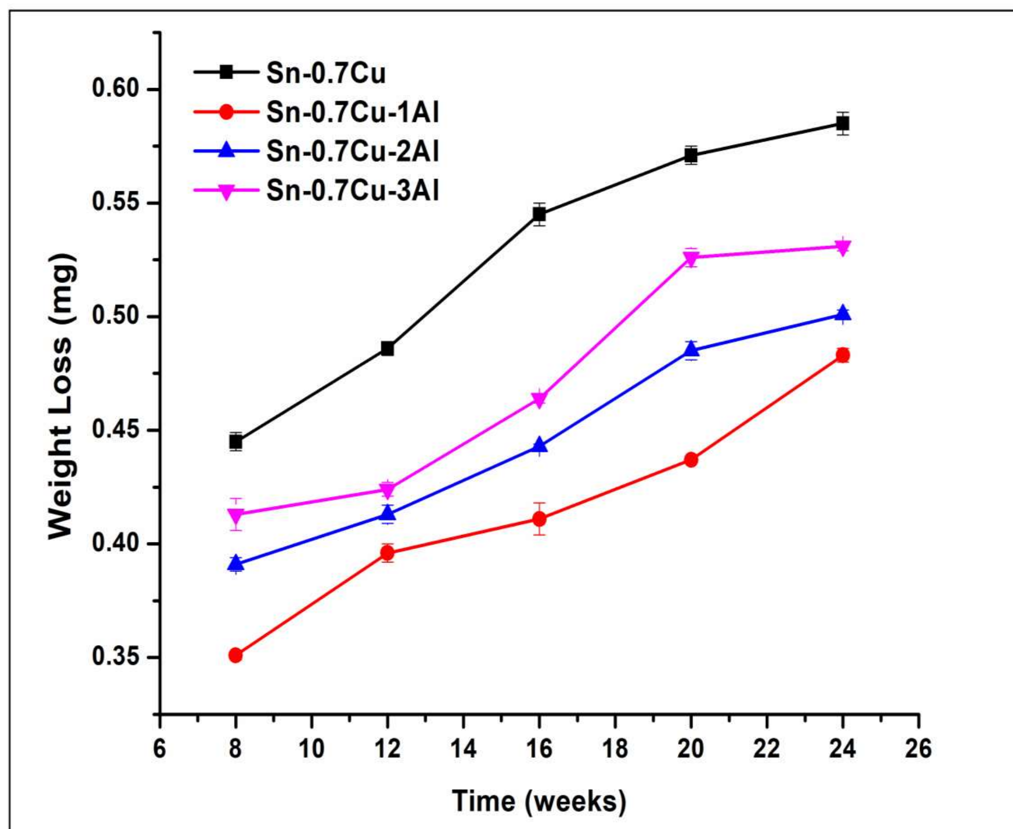

Fig.5. 3 Weight change of Sn-0.7Cu-xAl alloys after immersion in 3.5wt % NaCl at ambient temperature

Table 5. 3 Corrosion rate of Sn-0.7Cu-xAl solder alloy immersion in 0.5M NaCl

S. No.	Samples	Corrosion Rates * 10^{-4} (mm/yr)
1	Sn-0.7Cu	9.26 ± 0.016
2	Sn-0.7Cu-1Al	7.02 ± 0.017
3	Sn-0.7Cu-2Al	7.51 ± 0.019
4	Sn-0.7Cu-3Al	8.12 ± 0.013

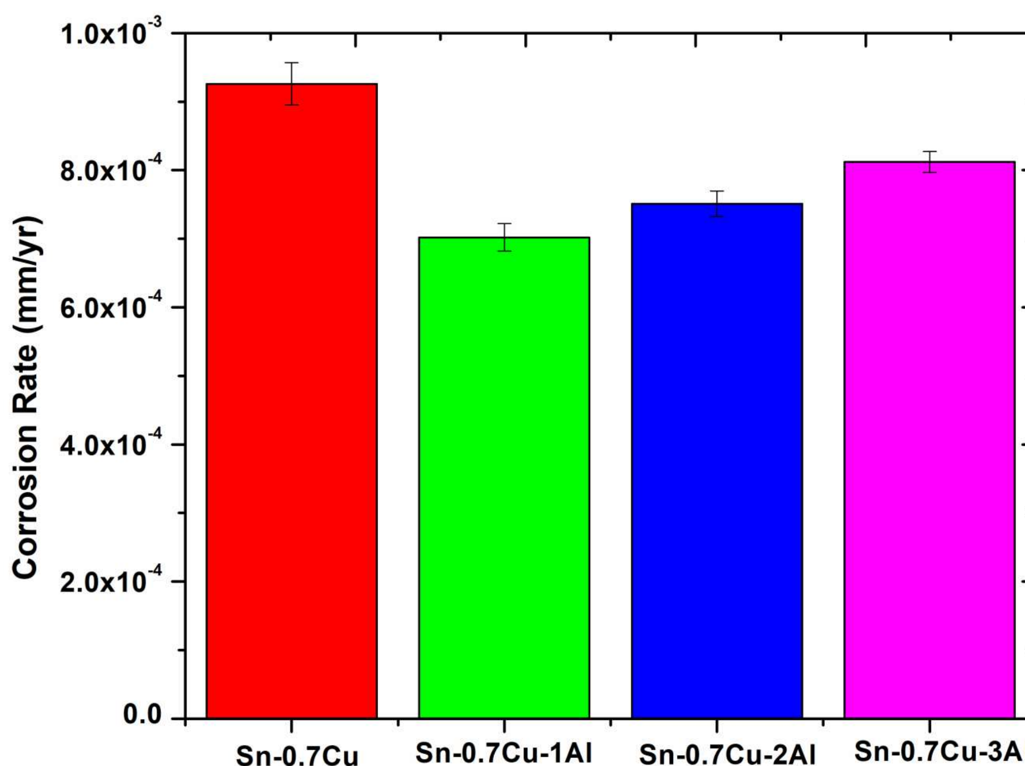

Fig.5. 4 Corrosion rate of Sn-0.7Cu-xAl alloys static immersion in 3.5 wt.% NaCl at ambient temperature

5.2.3 Potentiodynamic Polarisation Behaviour

The potential polarisation curve of Sn-0.7Cu-xAl ternary alloys in 3.5wt % NaCl solution is presented in Fig. 5.5. The exact electrochemical behaviour of various ternary will depend on the composition of the solder alloys. Take, as an example, the

potentiodynamic Sn-0.7Cu polarisation curve. The cathodic reaction stage is the AB region. The neutral solution's cathodic reaction is an oxygen reduction reaction connected to the laboratory atmosphere throughout the experiment.

$$O_2 + 4e^- + 2H_2O \rightarrow 4OH^- \quad (1)$$

Also, many hydrogen bubbles were found during the experiment, which other researchers have reported, corresponding to the evolution of hydrogen on the cathode[144][145][56].

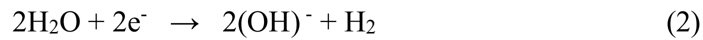

$$2H_2O + 2e^- \rightarrow 2(OH)^- + H_2 \quad (2)$$

The anodic reaction stages involve a few regions: BC, CD, DE, and EP. In general, the production of the passivation layer starts with the precipitation of $Sn(OH)_2$ on the surface from point B to point C. The building up of the corrosion products was monitored during the experiment. Sn active dispersion continues until a critical value of corrosion products is reached on the surface (at point C). As shown in the equation, such corrosion products cover the surface and prevent further corrosion of the alloy; a plateau region (CD) emerges on the curves.

The current density remains at approximately $-5A/cm^2$ with a relatively stable value. The passivization behaviour is presented in many states. The active dissolution of Sn, as shown in equations, is explained stepwise as follows:

$$Sn \rightarrow Sn^{2+} + 2e^- \quad (3)$$

$$Sn^{2+} \rightarrow Sn^{4+} + 2e^- \quad (4)$$

$$Sn + 2OH^- \rightarrow Sn(OH)_2 + 2e^- \quad (5)$$

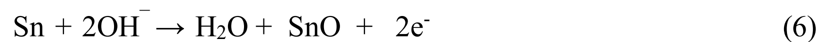

$$Sn + 2OH^- \rightarrow H_2O + SnO + 2e^- \quad (6)$$

$$Sn(OH)_2 \rightarrow H_2O + SnO \quad (7)$$

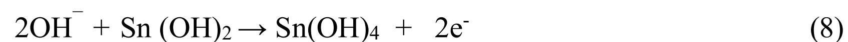

$$2OH^- + Sn(OH)_2 \rightarrow Sn(OH)_4 + 2e^- \quad (8)$$

$$H_2O + 2OH^- + SnO \rightarrow Sn(OH)_4 + 2e^- \quad (9)$$

$$Sn(OH)_4 \rightarrow SnO_2 + 2H_2O \quad (10)$$

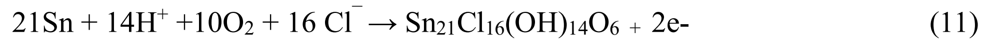

$$21Sn + 14H^+ + 10O_2 + 16\,Cl^- \rightarrow Sn_{21}Cl_{16}(OH)_{14}O_6 + 2e- \quad (11)$$

A rapid rise in current density is seen when a potential approaches D. This indicates an interruption of a protective passivation film due to the oxygen evolution reaction in Equation 5 and the absorption of Cl^- by the corrosion products[156]. Tin monoxide (SnO) is a semiconductor oxide that can diminish corrosion resistance. It is, thus, damaging to the stability of the passivation film. The results are a strong peak in line with the active dissolution generated by the Cl^- ions, resulting in the first pitting, which inevitably breaches the passivation layer consistency, with the $SnCl_3$ and $SnCl_6^{2-}$ soluble forming complexes. Thermodynamically stable tin oxide has been formed. It enables tin hydroxides to dehydrate quickly to create SnO_2 and SnO [157][158].

Table 5.4 summarises the relevant results of the polarisation test. The corrosion current density (I_{corr}) has been determined by extrapolating the cathodic Tafel area due to a well-defined investigation of the cathodic and anodic areas. The corrosion potential (E_{corr}) shifted from negative -879.29 to –463.12 mV to a more negative value. We are increasing the aluminum weight percentage from 1wt. % to 3wt. % in Sn-0.7Cu binary solder alloys, and the potential corrosion decrease with aluminum contents increase.

The value of corrosion potential (E_{corr}) exhibits a negative shift trend; a nobler value of E_{corr} suggests that thermodynamically the alloy is harder against corrosion. Thus, according to thermodynamics, 1 wt. Percent Al addition in binary Sn-0.7Cu solder alloy is easily found to improve its corrosion resistance. Given the current corrosion (I_{corr}) density with decreased Al addition, more than one magnetization, particularly with Sn-0.7Cu-1Al. Usually, Icorr is an essential metric for analyzing corrosion kinetics and is

generally used as the alloy corrosion rate at E_{corr}. Therefore, it is possible to conclude that the Al addition of Sn-0.7Cu alloy would decrease corrosion rates. Al has the best resistance to corrosion in the present work by 1 percent addition [119].

The smallest current density I_{corr} value indicates the highest corrosion resistance in passivation films. As Table 5.4 shows, the Sn-0.7Cu alloys decrease I_{corr} values after Al has been added, which means Al has improved the passivation film's protective effect. This outcome could be associated with the participation of Al in passiveness [159]. It can be concluded from the polarisation experiment that adding Al into the Sn-0.7Cu alloy could reduce the corrosion rate greatly; however, adding excess Al would adversely affect the corrosive resistance of the alloy.

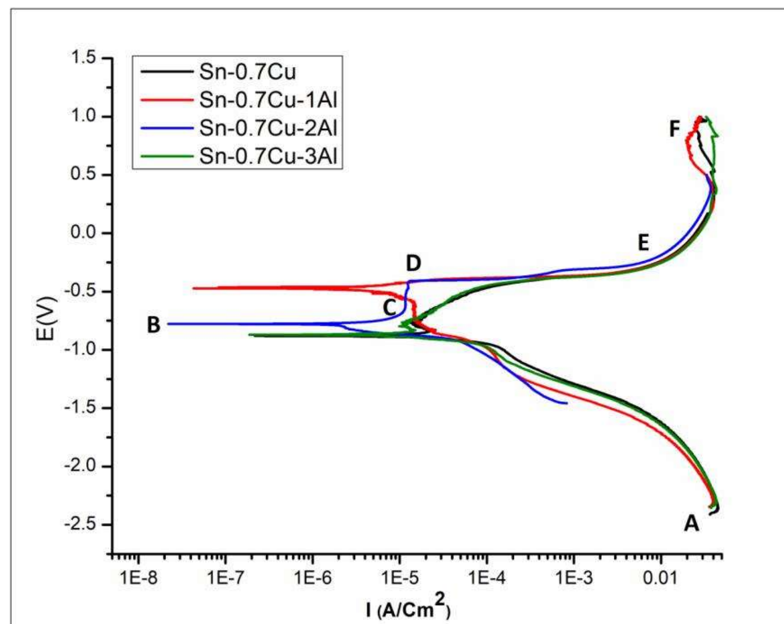

Fig.5. 5 Potentiodynamic polarization curve of lead-free Sn-0.7Cu-xAl solder alloys

Table 5. 4 Summary of Polazition parameters for Sn-0.7Cu-xAl lead-free solders alloys.

Samples	I_{corr} (µ Amps/cm^2)	E_{corr} (mVolts)	Corrosion Rate (mm/yr)*10^{-2}
Sn-0.7Cu	32.7500	-879.29	10.7030
Sn-0.7Cu-1Al	00.4908	-463.12	00.1604
Sn-0.7Cu-2Al	02.9798	-777.66	00.9738
Sn-0.7Cu-3Al	29.1740	-870.22	09.5340

5.2.3 Electrochemical Impedance Spectroscopy Analysis

Electrochemical spectroscopy (EIS) has been used to assess the resistance to corrosion at open circuit potential (OCP). Scattered Bode and Nyquist representations are illustrated in Fig. 5.6. All Al-containing Sn-0.7Cu alloys exhibit a straight line at a low-frequency area and are superimposed at an angle of around 45^0 at two axes, while the Sn-0.7Cu alloy shows the half-circular arc. It suggests that the kinetics of the corrosion mechanism due to the development of corrosion product for Sn-0.7Cu alloy changes to diffusion control processes in Al-mixing alloys called Warburg impedance. In other words, adding Al would change the mechanism for corrosion. The capacities in high-frequency regions are present in all the studied alloys. Of course, all the alloys studied have high-frequency capacity behaviour. The radius of the Sn-0.7Cu-1Al arc is the largest of the Al-containing alloys, which means that the Al-containing alloys have superior corrosion resistance to the Sn-0.7Cu alloy. In addition, in Fig. 5.6(c), two peaks in the curve indicate that two-time constants should be available at EIS. Further, the positions of those peaks for Al-containing Sn-0.7Cu solder alloys have changed compared to Sn-0.7Cu, which suggests that the electrochemical interface is different in dielectric behaviour.

Based on the above interpretation, two models for the EIS data of no Al-containing Sn-0.7Cu alloy and Al-containing Sn-0.7Cu solder alloys, respectively, are being used to adapt the EIS data shown in Fig. 5.7. Rs is the resistor to the solution; R_1 and CPE_1

indicate the resistance and the capacity of the product layer of porous corrosion; R_2 and CPE_2 indicate the resistors and capacities of the two layers between the corrosion product the alloy interfaces. W is the impedance of Warburg. CPE is carefully combined with distributed surface reactivity in homology, rawness, species adsorption, and electrode porosity[160].

Table 5.5 summarises the appropriate parameters of EIS data, and the Standard deviation assesses the quality of fitting results [161]. The suggested EEC models can quantitatively evaluate electrochemical compatibility with a high degree of accuracy. Given that this experiment was conducted with a single solution, assuming that all alloys have roughly the same R_s value is plausible. R_1 values of those alloys containing Al are several times greater than that of Sn-0.7Cu. As shown above, R_1 shows the resistance to corrosion of the layer of porous corrosion products. Therefore, it can be concluded that adding Al leads to producing a more protective product layer of corrosion. It is reasonable to conclude that the same solution in the experiment gives virtually the same value of R_s for all alloys. The value of R_1 of these Al alloys is many times higher compared to Sn-0.7Cu alloy.

The corrosion behaviour of a porous oxide layer is depicted in the previous illustration. On the basis of this, the addition of Al may result in the production of a layer of a much more protective corrosion product. Especially to be mentioned by increasing the content of Al, the R_1 value is slowly decreasing, which indicates that the addition of excess Al will lead to degradation of corrosion product protection capacity. In this work, an extended total resistance, $R_t= R_w + R_2 + R_1$ [146][147][162], is introduced to quantitatively analyze its corrosion resistance taking into account the presence of the Warburg impedance, and solution resistance Rs are omitted because it is essentially constant. Therefore, the total resistances Rt of Sn- 0.7Cu-xAl are calculated as 0.96, 12.89, 6.38,

and 1.73 Ω cm^2. The highest R_t is for Sn-0.7Cu-1Al solder alloys. Comparative analysis of the value of R_t above, the conclusion can be found that the addition of Al to Sn-0.7Cu alloy can improve the corrosion resistance and that too 1wt. % of Al in the present work is the optimum composition based on polarization and EIS test results.

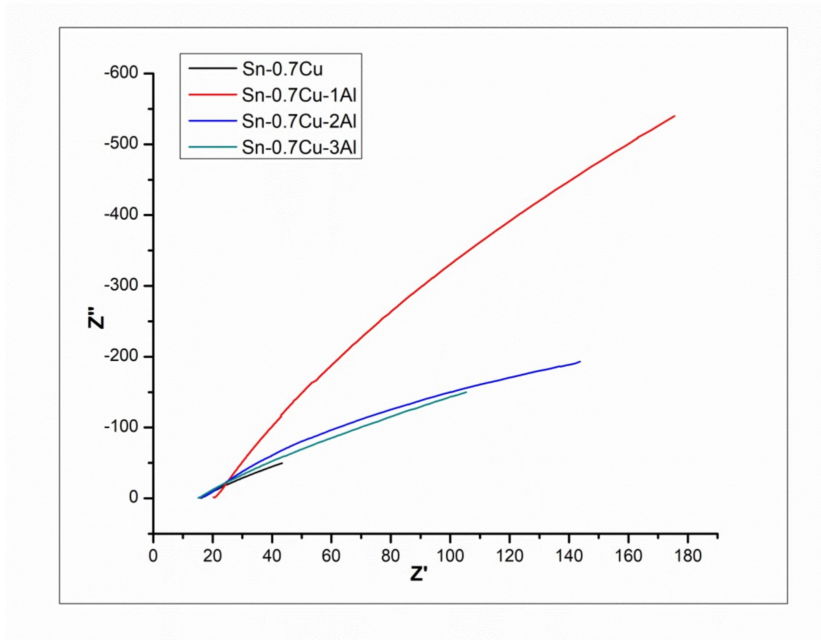

(a)

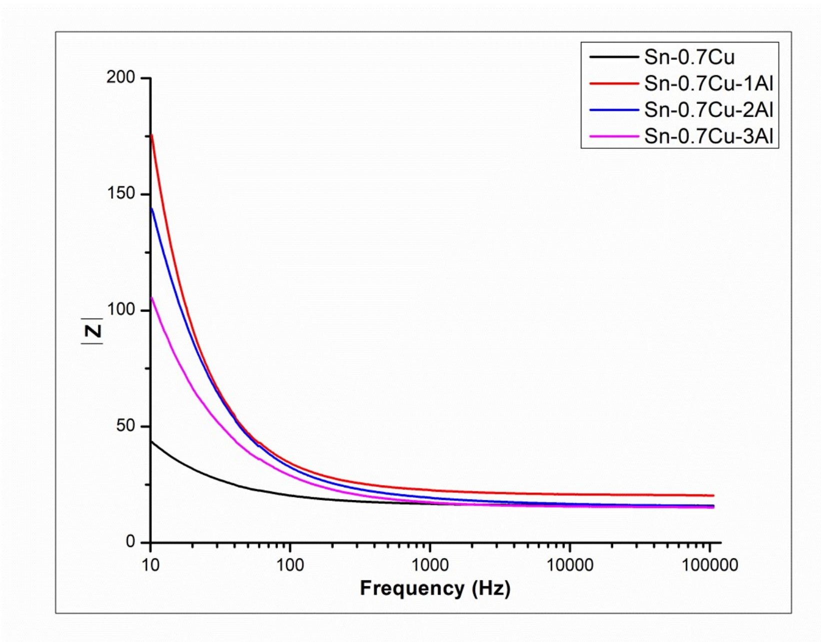

(b)

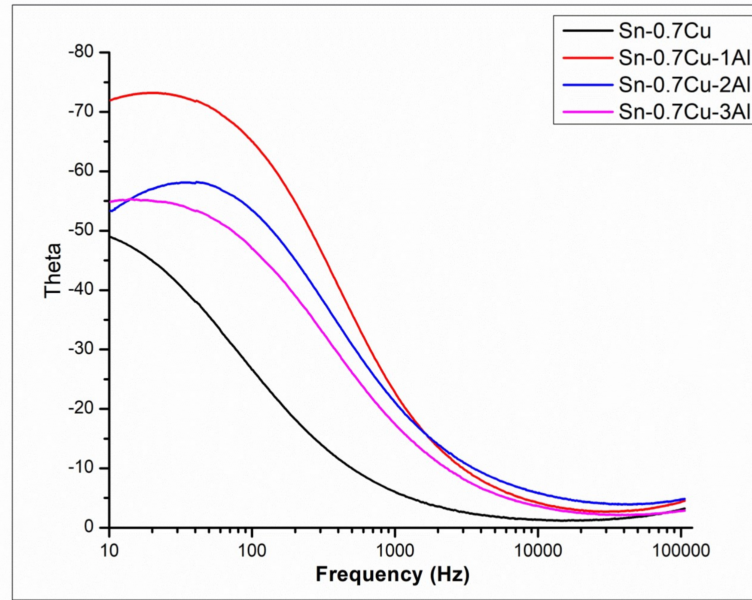

(c)

Fig.5. 6 Nyquist (a) and Bode plots (b,c) of Sn-0.7Cu-xAl solder alloys in 0.5M NaCl Solution.

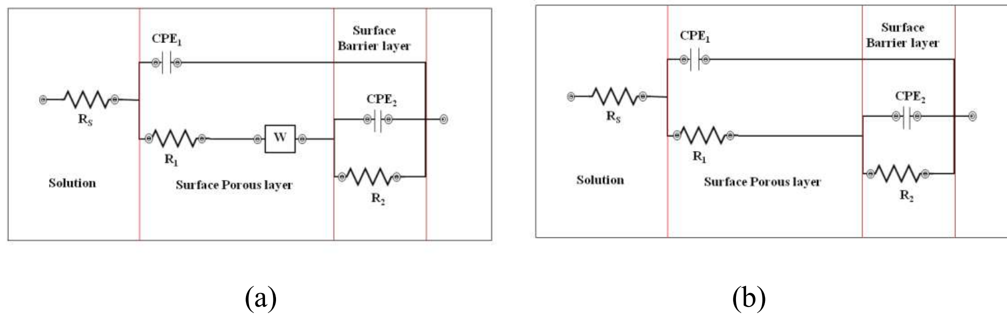

(a) (b)

Fig.5. 7Electric circuit models for fitting solder alloys (a) Sn-0.7Cu and (b) Sn-0.7Cu-xAl

Table 5. 5 Parameters of the Equivalent electrical circuit (EEC) model.

Samples	R_s Ωcm^2	R_1 Ωcm^2	CPE_1		R_2 Ωcm^2	CPE_2		R_w Ωcm^2	χ^2 * 10^{-4}
			Y_1*10^{-6} $\Omega cm^{-2}s^n$	n_1		Y_2*10^{-6} $\Omega cm^{-2}s^n$	n_2		
Sn-0.7Cu	16.04	344.6	644.54	0.76	624.1	817.24	0.72		12.655
Sn-0.7Cu-1Al	16.86	7840	43.072	0.89	5044	42.298	0.89	2.308	22.750
Sn-0.7Cu-2Al	16.18	5145	158.50	0.76	1235	173.78	0.74	3.501	64.912
Sn-0.7Cu-3Al	15.26	566.8	197.90	0.77	1168	248.3	0.73	3.267	4.8093

5.2.4 Characterization of Corrosion Products.

XRD and EDX were employed to assess the composition of solder alloys, while SEM determined the surface topography. The test was done before and after the electrochemical corrosion in 3.5wt.% of NaCl solution. Alloy surfaces are covered with platelet- and sponge-like structures such as branching crystallites.

Compounds that EDS and XRD have identified as tin oxide and other corrosion products have been identified. Sn–0.7Cu solders with an aluminum content variation of 0 to 3 wt% are shown in Fig. 5.6 to have a sponge-like structure of different sizes on their surfaces following corrosion. The Sn–0.7Cu–1Al sample shows a higher density of sponge-like structures than the Sn–0.7Cu, Sn-0.7Cu-2Al, and Sn-0.7Cu-3Al solder alloy. The corrosion products Sn–0.7Cu and Sn–0.7Cu–1Al are similar in morphology and quantity. According to expectations, corrosion products on the surface alloys should have more continuous and refined properties than those on the corroded surface alloys. For this reason, a dense product layer on Sn–Cu–Al alloys is beneficial in enhancing their corrosion resistance.

In order to determine the corrosion products, all alloys utilized in this research were subjected to EDX analysis, as shown in Fig. 5.9. O, Na, Cl, Cu, and Sn are present in significant quantities on the surface of the alloys following corrosion, although the Al weight percent was substantially the lowest of all. It is more likely that the corrosion products will contain $Sn_{21}Cl_{16}(OH)_{14}O_6$ on the alloy surface as an actual product, often associated with minor amounts of oxide compounds. An X-ray diffractometer (XRD) was used to determine the phase composition of the corrosion products. Fig. 5.10 shows the XRD pattern of the corroded samples with an aluminum variation. Major phases formed during the corrosion were $Sn_{21}Cl_{16}(OH)_{14}O_6$ and other minor phases such as SnO, SnO_2,

and Al_2O_3. Chloride in $Sn_{21}Cl_{16}(OH)_{14}O_6$ can be explained by the existence of a higher amount of Sn at the surface of metal alloys, as seen in Fig. 5.10. The intensity of Al_2O_3 increases with the increasing aluminum content of the alloy. It is more likely that the corrosion products will contain $Sn_{21}Cl_{16}(OH)_{14}O_6$ on the alloy surface as a significant product, generally paired with modest quantities of oxide compounds [56].

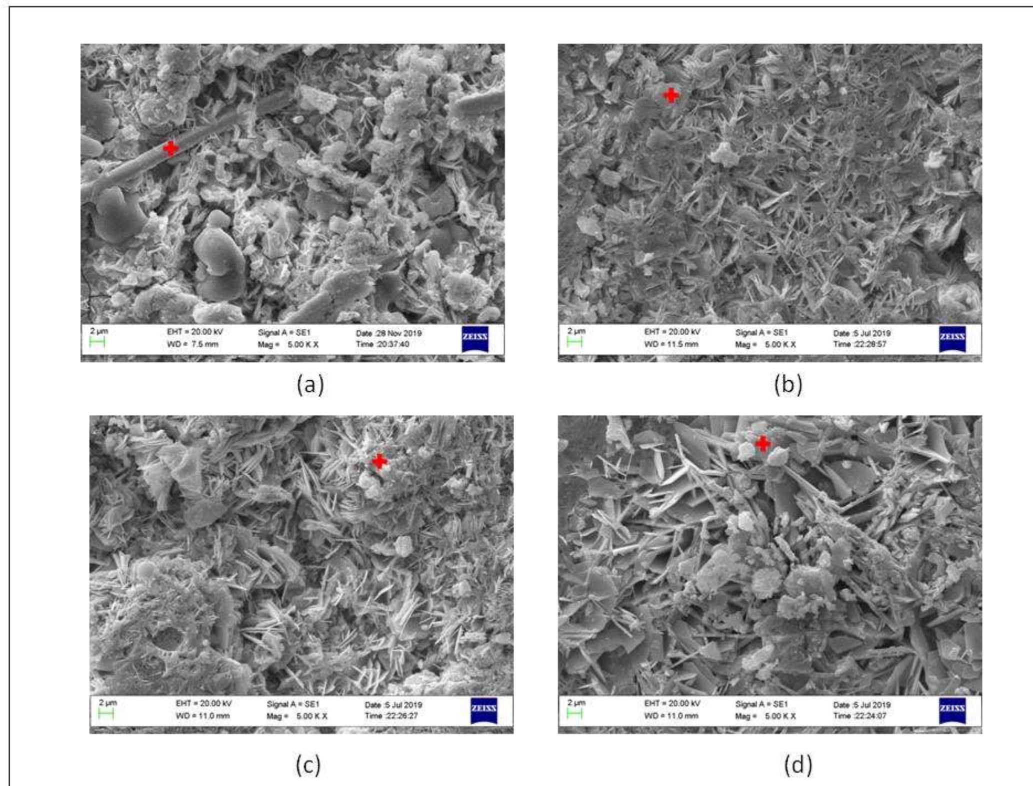

Fig.5. 8 *Surface morphology (SEM) of corroded surfaces of solder alloys (a) x=0, (b) x=1, (c) x=2 and (d) x=3*

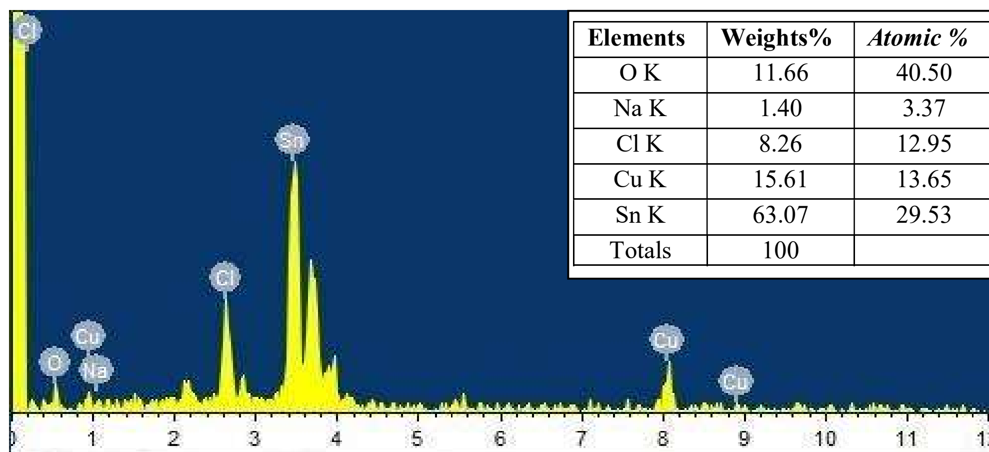

Elements	Weights%	*Atomic %*
O K	11.66	40.50
Na K	1.40	3.37
Cl K	8.26	12.95
Cu K	15.61	13.65
Sn K	63.07	29.53
Totals	100	

(a)

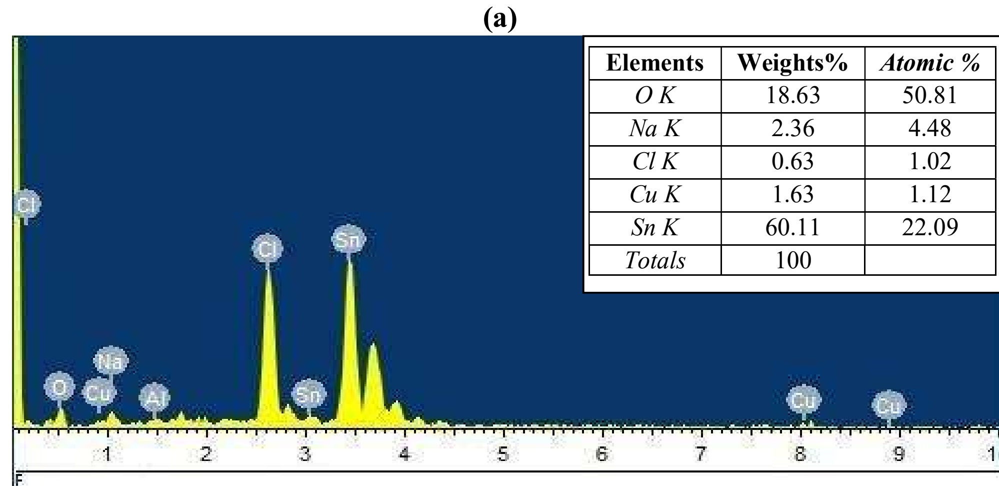

Elements	Weights%	*Atomic %*
O K	18.63	50.81
Na K	2.36	4.48
Cl K	0.63	1.02
Cu K	1.63	1.12
Sn K	60.11	22.09
Totals	100	

(b)

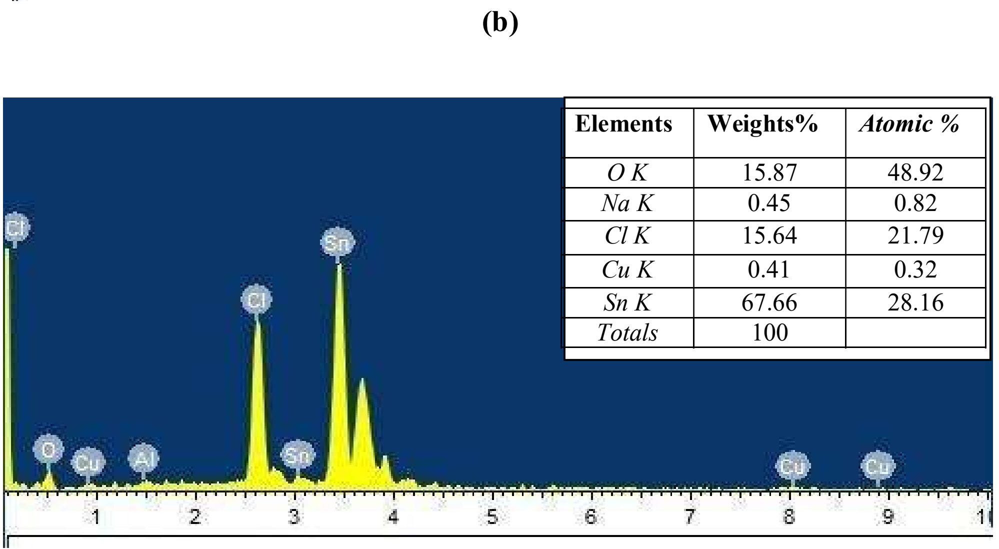

Elements	Weights%	*Atomic %*
O K	15.87	48.92
Na K	0.45	0.82
Cl K	15.64	21.79
Cu K	0.41	0.32
Sn K	67.66	28.16
Totals	100	

(c)

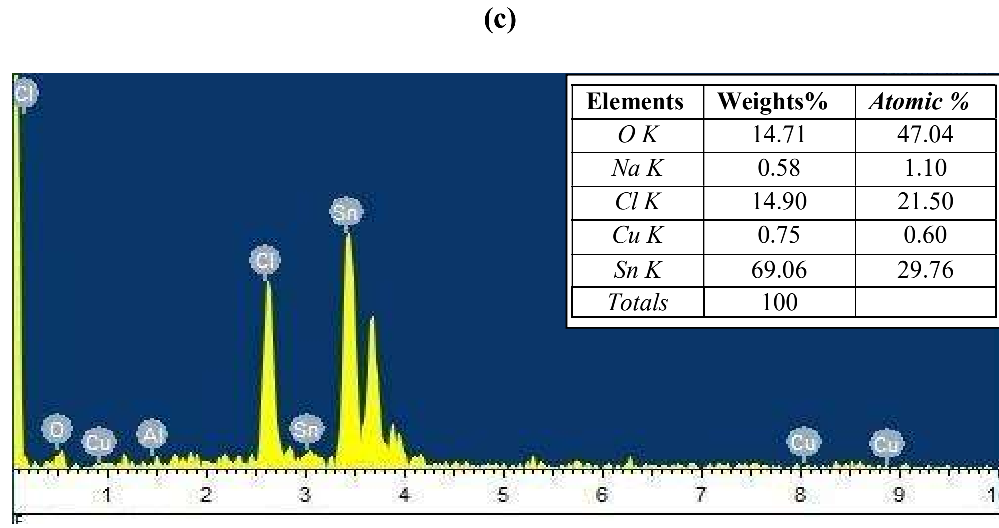

Elements	Weights%	*Atomic %*
O K	14.71	47.04
Na K	0.58	1.10
Cl K	14.90	21.50
Cu K	0.75	0.60
Sn K	69.06	29.76
Totals	100	

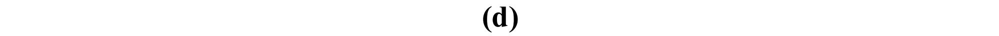

(d)

Fig.5. 9 EDX of corrosion products of Sn-0.7Cu-xAl solder alloys (a) x=0, (b) x=1, (c) x=2 and (d) x=3.

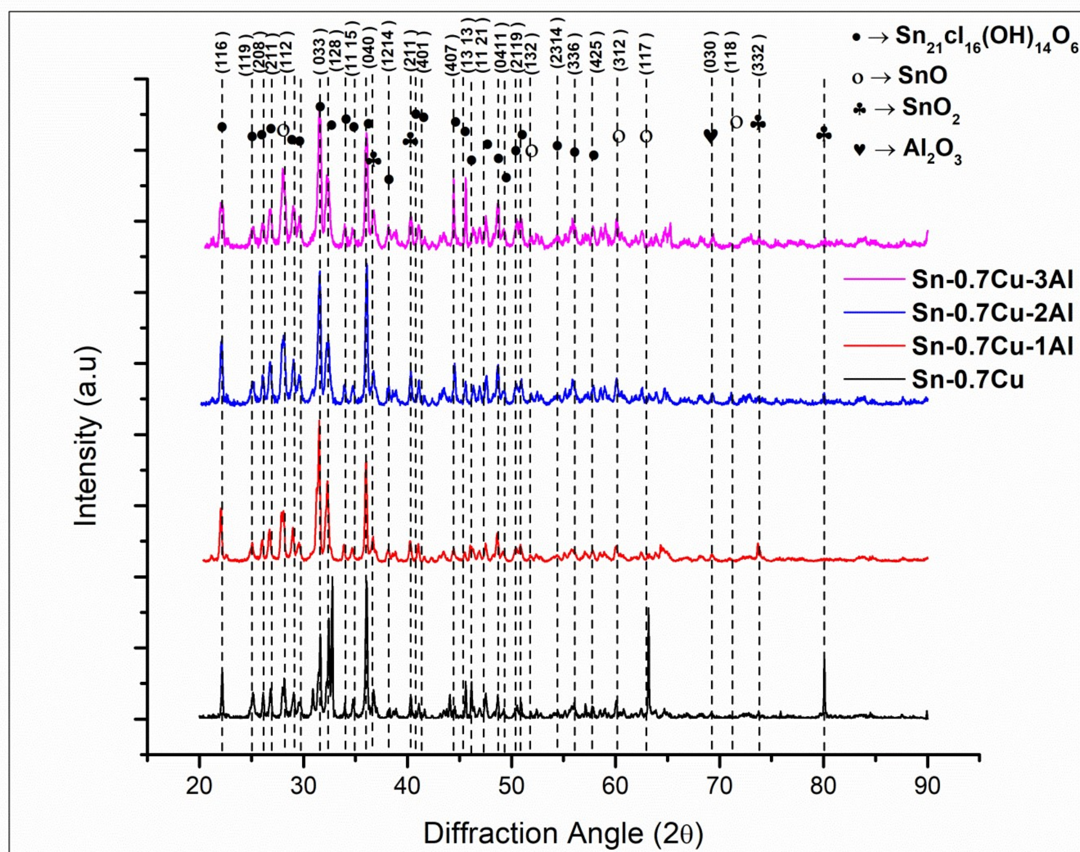

Fig.5. 10 XRD pattern of corroded Sn-0.7Cu-xAl

5.2.5 Corrosion Mechanism

Most corrosion is characterized by surface layer breakdown followed by pitting corrosion. Al-rich precipitate acts as a surface layer in this case. After initial Al-rich deposits, Cl^- has migrated into the alloys showing that Cl transport is selective and Al is dissolved preferentially. Corrosion-alloy interfaces can be seen in this image. Between Al-rich precipitates and Sn matrix, pores and micro-cracks may be seen along the intergranular boundaries between the precipitates and matrix[150]. It may be seen that there is a localized breakdown at the interface between the corrosion products and the alloy. Al-rich precipitates are separated from the Sn matrix by a thin layer of intergranular pores. By penetrating an oxide layer's intergranular borders with an easily adsorbable anion like Cl^-, a localized breakdown of the film can be triggered, followed by pitting or passivation of

the metal/oxide interface. A pitting mechanism that takes Cl^- into account is utilized to evaluate the pitting development of Sn–0.7Cu alloys.

Stage I: Cl^- adsorbs first into oxide intergranular boundaries where its activation energy should be many orders of magnitude higher than bulk adsorption. Instead, Sn oxides grown on alloys behave like n-type semiconductors, indicating that the oxide film and the solution have a positively charged interface. As a result, chlorine adsorption into the film is facilitated. Because chloride complexes are more easily generated when Cl^- is coupled with Sn^{4+}/Sn^{2+}, the activation energy for the transfer to a solution is likewise reduced. As shown in Fig. 5.11, As seen in stage II, microscopic fractures occur on the passive film surface due to these properties extending towards the film/alloy contact. Cl^- migrates to the film-alloy connection to create chloride complexes. Because of volume expansion, the continual development of these complexes causes internal strain at the interface, culminating in localized collapse and pit formation at the initial Sn sites. This reaction is expected to occur during the repassivation process at the breakdown sites related to the transport of OH^- (also known as pitting inhibitory anion)[74]. Stage III, the increase in the concentration of these ions in the vicinity of the pits, results in inhibition of the growth of the pit. As the dissolution of metal ions proceeds, transversely pit growth takes place. Diffusion of OH^- ion into the pits resulted in decreased positive ions or acidity activity. This will result in a constant pit growth rate, and this stage is known as stage III, as shown in Fig. 5.11.

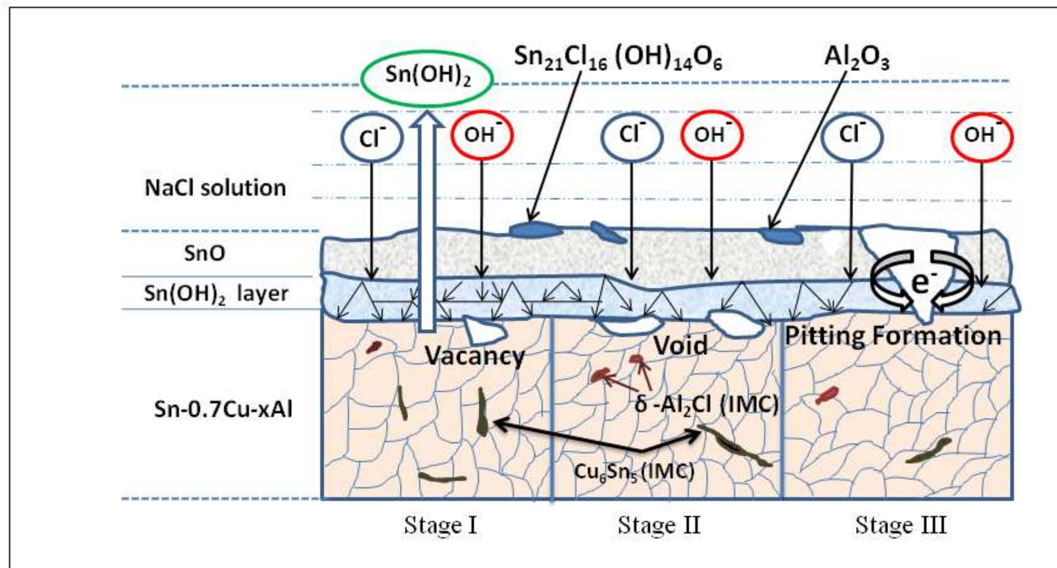

Fig.5. 11 Corrosion Mechanism of Solder alloys

5.3 Conclusions

Sn-0.7Cu-xAl solder alloys have been studied electrochemically in a neutral 3.5 wt.% NaCl solution using potentiodynamic polarization and EIS measurements. Metallographic characterization like SEM, EDXA, and XRD have been conducted to determine the effect of Al content on corrosion properties and optimize the composition of Sn-0.7Cu-xAl solder alloys from a corrosion standpoint. We can take a few conclusions from this.

1. As a result of adding Al to the Sn-0.7Cu alloy, the microstructure of corrosion products on the surface of solder alloys would alter. The kinetic characteristics of the corrosion product layer would shift from the charge transfer control process to the diffusion control process.
2. The inclusion of Al refines the coarse primary Sn phase and generates a homogeneous eutectic microstructure, which increases corrosion resistance. Sn-0.7Cu-1Al has a superior corrosion resistance than Sn-0.7Cu-2Al and Sn-0.7Cu-3Al.

3. When Al is an addition to Sn-0.7Cu alloys of more than 1%, Al_2Cu IMCs can be produced and validated as Al_2Cu. Those IMCs would break the corrosion product layer's continuity, causing pitting and reducing the corrosion resistance of Sn-0.7Cu alloys due to their presence.
4. To prevent the formation of IMCs, the Al percentage in Sn-0.7Cu-xAl alloys should be kept below 3wt% Al to prevent corrosion. The best composition in this study is 1wt% Al.